

# Debris Flow due to the Seepage-Induced Failure of a Granular Pile

Hsien-Ter Chou

*Professor, Dept. of Civil Engineering, National Central University, Chung-Li, Taiwan, R.O.C.*

*Email: htchou@cc.nc.edu.tw*

Ching-Fang Lee,

*Associate Researcher, Disaster Prevention Technology Research Center, Sinotech Engineering Consultants, Inc., Taipei, Taiwan, R.O.C., E-mail: cflee@sinotech.org.tw*

Yi-Hong Tu

*Master, Dept. of Civil Engineering, National Central University, Chung-Li, Taiwan, R.O.C.*

*Email: htchou@cc.nc.edu.tw*

Su-Chin Chen

*Professor, Department of Soil and Water Conservation, National Chung Hsing University, Taichung, Taiwan, R.O.C. Email: scchen@nchu.edu.tw*

**ABSTRACT:** The mobilization process of a granular pile and the associated debris flow by the action of upstream runoff and seepage was experimentally investigated in an inclined flume. The critical condition and the failure process of the granular pile were analyzed by employing the PTV approach. The effect of runoff discharge, flume slope and permeability are explored. During the mobilization process, a partially unsaturated granular snout was formed, then became a bulge at the surge front just as stony debris flows in the field. The velocity profile in the unsaturated snout depicts a Bagnold's rheology, but it deviates slightly from Bagnold's profile due to presence of bottom slipping in the intermediate saturated zone. In addition, the evolution of solid fraction indicates that the critical failure condition is controlled by the seepage flow. A dimensionless peak debris surge related to the chute slope is also presented.

**KEY WORDS:** debris flow, seepage flow, runoff, granular pile, Bagnold's rheology.

## 1 INTRODUCTION

Debris flows are mainly caused by (1) liquefaction of landslide blocks, (2) failure of landslide dams, or (3) mobilization of the gully bed by surface water flows (Takahashi, 1991). Among those scenarios, debris flows due to the failure of landslide dams may induce catastrophic disasters because the magnitude of the bursting debris flood is far larger than the runoff. Dam-break induced debris flows are classified by (1) overtopping, (2) sliding and (3) progressive failure (Takahashi and Kuang, 1998). The surging behavior of debris -flow snouts is a function of channel slope and flow velocities, which has been explored by employing the tilted conveying belt experiments (Davies, 1990), and numerical and theoretical analysis (Berzi and Jenkins, 2009). A recirculated zone near the snout was observed in the experiments (Hsu *et al.*, 2008). The granular-liquid mixture over a mobile bed with different saturation levels and slopes was experimentally examined (Fracarollo *et al.*, 2007).

This study experimentally examines the sliding process of a granular pile due to seepage failure and the subsequent debris flow, *i.e.*, corresponding to the Type (2) dam-break induced debris flow defined by Takahashi and Kuang (1998). Such situations may occur when a loose landslide blocked the steep ravine with moderate upstream runoff seeping through the landslide dam temporarily prior to its failure. The effect of channel bed entrainment is neglected for simplicity. Both the slip process and the formation of the debris flow are examined. Especially the snout profiles and the peak surge flows under different slopes and inflows are explored. Such information is helpful for countermeasures or downstream warning systems.

## 2 EXPERIMENTAL SETUP AND PROCEDURES

An adjustable inclined flume with transparent glass plates on both sides, being in the dimension of 2.05 m ( $L$ ) x 0.12 m ( $W$ ) x 0.6 m ( $H$ ), is used to examine the failure and mobilization process of a granular pile under the action of upstream runoff (Fig. 1). A constant head tank on the upstream provides a steady unit discharge of 16-25 cm<sup>2</sup>/s, while the chute slope is within the range of 6°-18°. The granular pile consists of uniform polystyrene beads ( $d=0.6$  cm,  $\phi=20.8^\circ$ ,  $\rho=1.915$  g/cm<sup>3</sup>), which were also compactly glued on the chute bottom in a single layer to serve as the rigid bed. The effect of bed entrainment thus is neglected. In the observation zone, a mirror installed on the side wall with an included angle of 45° provides the synchronous top view by reflection. A high-speed CCD camera (IDT Motion Pro X3) with a sampling rate of 400 fps is installed close to the side wall of the downstream chute to capture both the side-view and top-view images. The capture region is illuminated by two continuous halogen lamps at both end-walls. Particle tracking velocimetry (PTV) based on the Voronoi cell method are utilized to make velocity measurements with high spatial and temporal resolutions (Capart *et*

al., 2002).

Each center of particle at  $t_i$  will be registered systematically and compared with the previous stage ( $t_{i-1}$ ), so that the velocity vector at the transient time can be evaluated. In order to reduce the velocity fluctuation, all the transient velocity vector is averaged per ten frames to obtain a mean value in each grid mesh. In Generally, the length unit on the image (pixel) and real chute (ex. cm) is different. The calibrated length scales for both side-view and top-view images are 1(cm):27.36(pixel) and 1(cm):25.21(pixel), respectively. The profile of flow rate of granular flow in the observation zone are also estimated from the depth-integration at specific horizontal position.

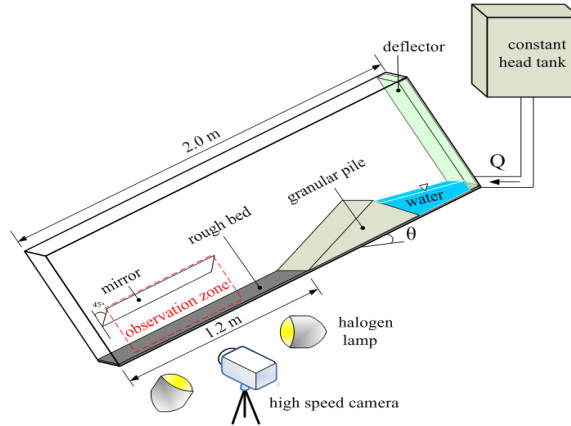


Figure 1 Experiment setup for the mobilization process of a granular pile

### 3 RESULTS AND DISCUSSION

#### 3.1 Failure process of the granular pile

The triangular granular pile under the actions of upstream runoff ( $q_w=25\text{cm}^2/\text{s}$ ,  $\theta=15^\circ$ ) and seepage forces become unstable in a short instant (less than 1s as shown in Fig.2 ). As the downstream slope movement is clearly observable at  $t=1\text{s}$ , the upstream water stage is still lower than the peak of the pile and the upstream slope remains static. So the slide of the granular pile is due to the effect of seepage and water pressure instead of overtopping. As the deformation of the downstream slope evolves farther to the extend that the upstream water surface reach the pile peak at  $t=1.5\text{ s}$ , the whole pile starts moving. During its accelerating movement ( $t=2\text{-}4\text{ s}$ ), the downstream side of the pile moves faster than the upstream side and the granular body elongates. Consequently, the peak height of the snout decreases further with the increasing velocity. The debris-flow snout is clearly seen since  $t=2.5\text{ s}$ .

As one can see from the long-exposure images as shown in Fig. 3, the granular pile becomes unstable when the upstream water level reaches about one third of the upstream surface. The solid lines depict the seepage front while the dashed lines represent the slip surface. The slip surface is initiated from the front edge of seepage front, i.e. the bottom slip surface occurs within the saturated zone where the pore water pressure enhances the slope instability.

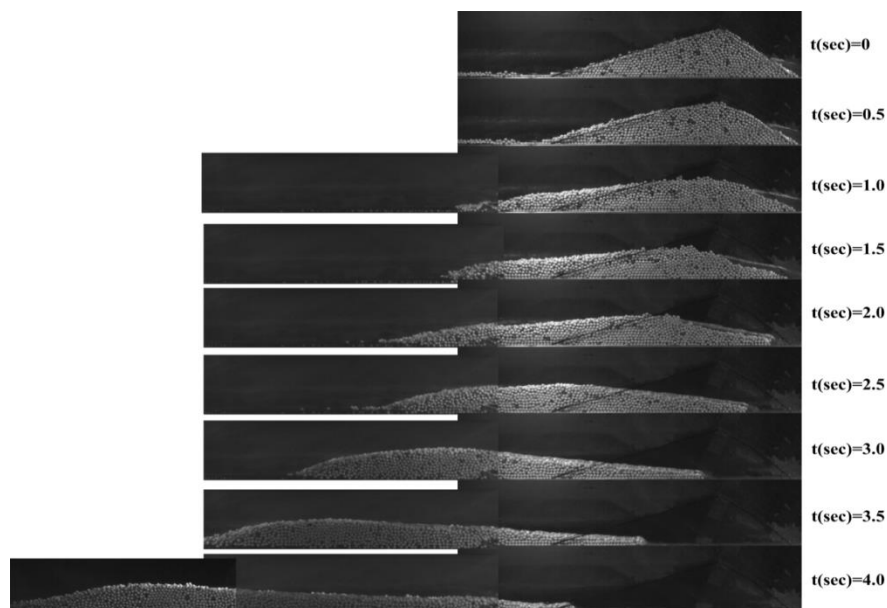
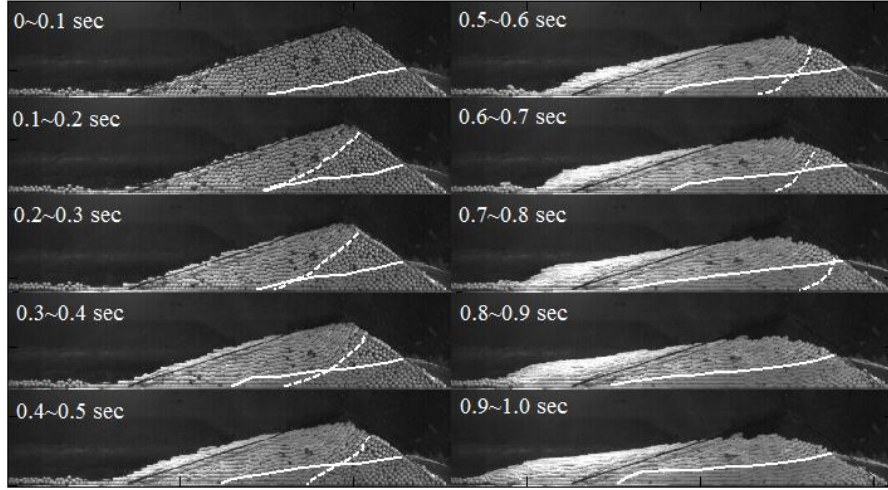
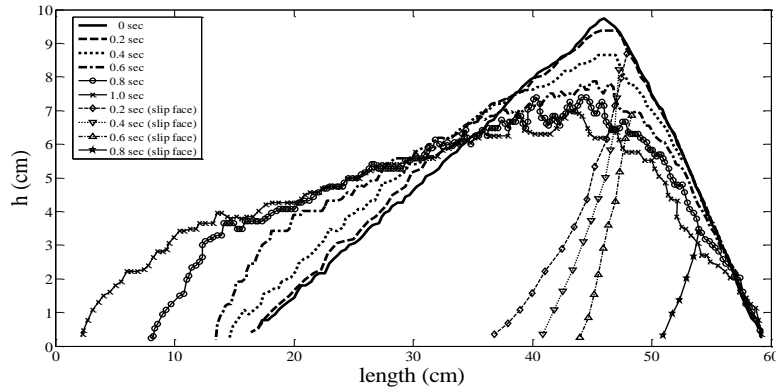


Figure 2 The failure process of a granular pile under the action of runoff and seepage ( $q_w=25\text{ cm}^2/\text{s}$ ,  $\theta=15^\circ$ )



**Figure 3** Long exposure of the slip process of the granular pile  
 $(q_w=25 \text{ cm}^2/\text{s}, \theta=15^\circ)$

As shown in Fig. 4, the slip surface then propagates upstream quickly. At  $t=0.4\text{s}$ , the drop of the pile peak is about 1.0 cm, and the collapsed particles move in the downstream direction. At  $t=0.8 \text{ s}$ , the drop rate of the granular peak declines but the evolution of downstream slope becomes more obvious. At time  $t=1\text{s}$ , the seepage line is almost parallel to the downstream slope. Even the downstream slope of the pile continues its deformation, the upstream side still not in motion since the water stage is still less the peak elevation at this moment (see Fig. 3).



**Figure 4** The tracked front edges and slip surface at different time interval( $q_w=25 \text{ cm}^2/\text{s}, \theta=15^\circ$ )

### 3.2 Side-view velocity profiles

For each experimental run, 11 successive frames were acquired to determine the ensemble results. The flow image measurements based on pairing Voronoi cells have been applied to explore both the side-view and top-view velocity profiles(Capart *et al.*, 2002). The sub-pixel accuracy was checked by fitting a quadratic surface to the neighborhood of its maximum. The center positions of particles are determined according to the surface peaks on the image. The side-view velocity profiles (at the slope of  $15^\circ$ ) at the peak for different flow rates are shown in Fig. 5. The Bagnold-type velocity profile is represented by the rigid curve, which is in the form as follows

$$u(y) = u_h[1 - (1 - y/h)^{3/2}] \quad (1)$$

where  $u_h$ =surface velocity,  $h$ =flow depth,  $y$ =elevation(from the chute bed). Most data points roughly follow the Bagnold profile, while the deviation is obvious within the regime of  $0.2 < y/h < 0.6$ . It is also noted that the slip velocity occurs for the particles near the bed, being with the magnitude of  $0.1\text{-}0.4 u_h$ .

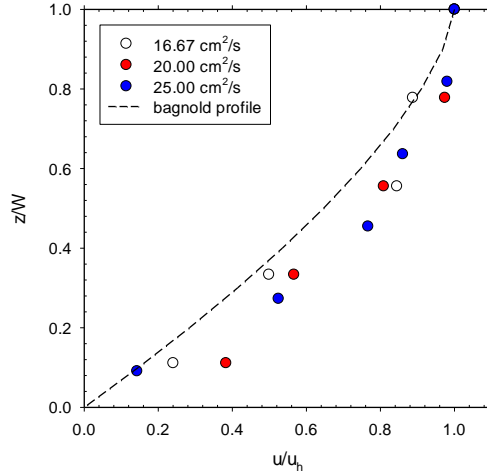
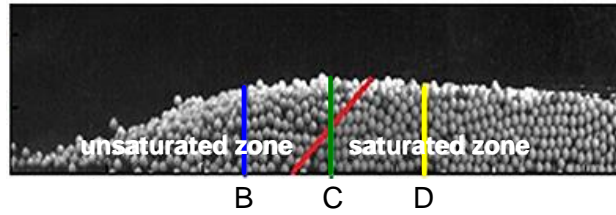
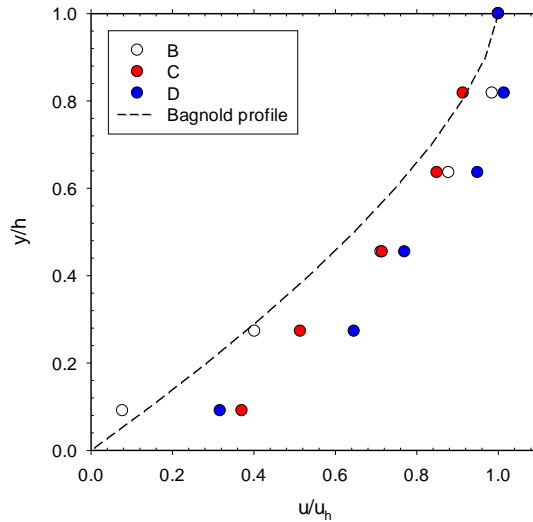


**Figure 5** Dimensionless velocity profile at the snout ( $\theta=15^\circ$ )

As shown in Fig. 6a, the front part of the debris-flow snout is unsaturated, and the inclined wetting front (about  $45^\circ$ , as shown by the red line) is located around the snout peak (Section C). So the peak itself is about half saturated, and it is followed by saturated granular particles. Sections B, C, and D are separated by 200 pixels, and their velocity profiles are shown in Fig. 6b. The unsaturated front (Section B) exhibits smallest slip velocity, and fits better for the Bagnold profile. While the half saturated and saturated zone (Sections C, D) are with larger slip velocities and are more deviated from the Bagnold profile.



(a) location of the observation (side view)



(b) velocity profiles

**Figure 6** Velocity profiles near the debris snouts ( $q_w=25 \text{ cm}^2/\text{s}$ )

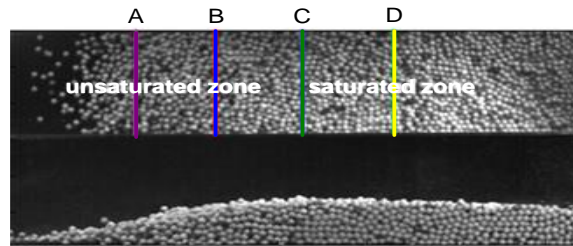
### 3.3 Top-view velocity profiles

The lateral velocity profiles from the top view were taken at 4 sections A, B, C, and D (with the interval of 200 pixels apart) as shown in Fig. 7a. The convex lateral velocity profiles show the difference of the surface particle velocities at the centerline and the wall are about 20-30 %. Especially for the front part, which is unsaturated and is with smaller particle

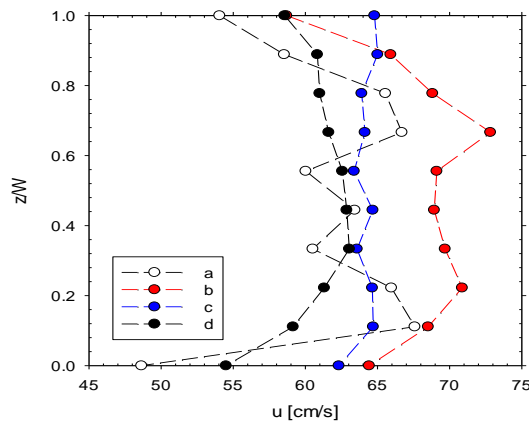
velocity due to its impingement with the chute bed. Two sections B and C near the peak exhibits the faster velocity. As shown in Fig. 7b, the wall friction effect is more obvious for the unsaturated zone than the saturated zone. The velocity distribution is similar to previous study carried out by Jop *et al.* (2005). The particle recirculated pattern near the snout proposed by Davis (1991) can also be explained by the longitudinal velocity difference at different sections.

### 3.4 Surge and saturation hydrographs

The granular flow surges and hydrographs of the water level at a given location near the snout for the cases ( $q=25 \text{ m}^2/\text{s}$ ) are shown in Fig. 8. The front part of the snout is unsaturated and the water level abruptly increases to the granular surface near the location of the granular peak. Behind the granular peak, most region is saturated. Comparing the hydrographs shown in Figs. 8a and 8b, one observes the rising speed of water level declines with the increasing slope. The increasing slope enhances the effect of gravity force, so the granular particles move faster and the snout extends a more elongated shape. The water follows behind the snout and makes the snout front be unsaturated.

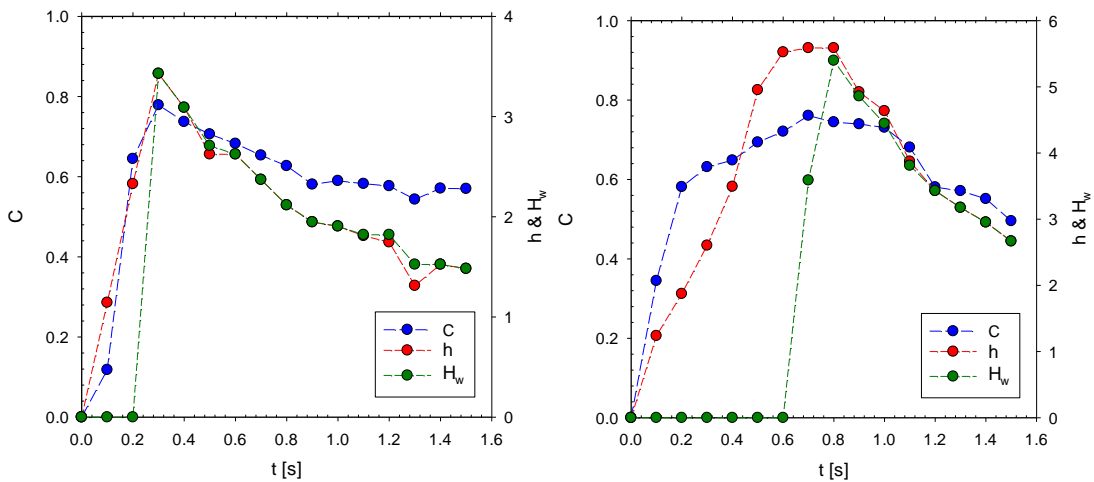


(a) Observation location (top and side views)



(b) Lateral velocity profiles

Figure 7 Lateral velocity profiles near the snout ( $q_w=20 \text{ cm}^2/\text{s}$ )



(a)  $\theta=9^\circ$

(b)  $\theta=15^\circ$

Figure 8 Saturation and hydrograph at a given location near the snout ( $q_w=25 \text{ m}^2/\text{s}$ )

### 3.5 Peak discharge relationship

The crucial parameter for the landslide-dam induced debris flow is the peak flow at a specific location. Here we summarized the experiental data for peak debris flow rates at the observation zone after the mobilization of the given granular piles under the conditions of different slopes and different inflows. As shown in Fig. 9, the dimensionless peak granular discharges (debris surges), being defined as  $q_p/q_w$ , is well related to the chute slope and in the form as follows:

$$\frac{q_p}{q_w} = \alpha(\sin\theta)^\beta \quad (2)$$

where  $q_p$  and  $q_w$  stand for peak flow rates and runoff, respectively,  $\theta$  = chute slope. According to the experimental data, the coefficients read  $\alpha = 86.3, \beta = 1.48$ . Further data would be needed in the future study to check its applicability.

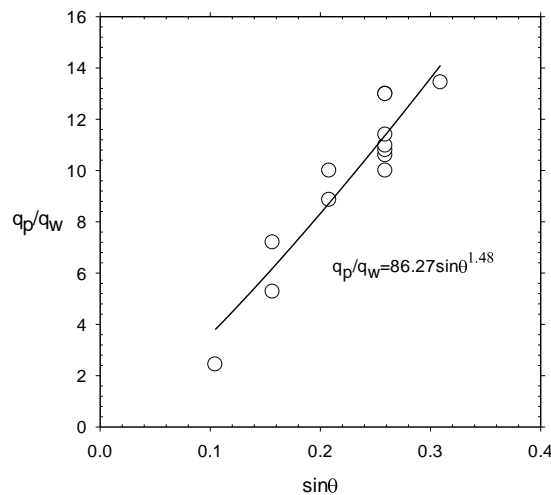


Figure 9 Dimensionless debris peak discharges versus slopes

## 4 CONCLUSIONS

The sliding process of a granular pile due to seepage failure and the subsequent debris flow is experimentally explored in this study. The slip surface is initiated front the wetting front near the bed and within the saturated zone without overtopping. During the subsequent debris flow, the front of the snout is unsaturated and the velocity roughly follows the Bagnold profiles. While the half saturated and the saturated zone near the peak are with a bottom slip velocity of 0.1-0.4 (relative to the surface velocity) and are more deviated from the Bagnold profiles. The convex lateral velocity profiles depicts the difference of the surface particle velocities between the centerline and the wall are about 20-30 %. The surface velocity sections near the peak exhibits the faster velocity than the snout front, which implies a recirculated pattern near the snout as proposed by Davis (1990).

The peak debris flow rates versus the upstream runoff at the observation zone is well related to the chute slope in the form of  $q_p/q_w = 86.3 \sin\theta^{1.48}$ . Further effects of the landslide characteristics such as the block volume and particle sizes on the debris flows deserve further studies.

## ACKNOWLEDGEMENT

The study is supported by the National Science Council, Taiwan, R.O.C. (NSC- 101-2811-M-008-062).

## References

- Berzi, D., and J. T. Jenkins, 2009, Steady Inclined Flows of Granular-Fluid Mixtures, *J. Fluid Mech.* Vol. 641, pp. 359-387.
- Capart, H., D. L. Young and Y. Zech, 2002, Voronoï Imaging Methods for the Measurement of Granular Flows, *Experiments in Fluids*, Vol. 32, pp.121-135.
- Davis, T.R.H.,1990, Debris-Flow Surges Experimental Simulation, *Journal of Hydrology (N.Z.)*, Vol. 29, No. 1, pp.23-46.
- Fraccarollo, L., M. Larcher and A. Armanini, 2007, Depth-averaged relations for granular-liquid uniform flow over mobile bed in a wide range of slope values, *Granular Matter*, 9:145-157 .
- Hsu, L., W. E. Dietrich and L. S. Sklar, 2008, Experimental Study of Bedrock Erosion by Granular Flows, *Journal of Geophysical Research*, Vol. 113, F02001.
- Jop, P., Y. Forterre and O. Pouliquen, 2005, Crucial Role of Sidewalls in Granular Surface Flows: Consequences For the Rheology, *J. Fluid Mech.*, Vol. 541, pp. 167-192.
- Takahashi, T. and S. F. Kuang,1988, Hydrograph prediction of debris flow due to failure of landslide dam: *Annuals, DPRI*, 31B-2: 601-615 (in Japanese).
- Takahashi, T. , 1991, *Debris flows*, IAHR Monograph Series, Rotterdam: Balkema.